Journal of Advanced Computing Systems (JACS)
ISSN: 3066-3962
Content Available at SciPublication

An Integrated Graph Neural Network and Reinforcement Learning Framework for Intelligent Drug Discovery

Chuan Wu[1], *Zhenghao Pan*[1,2]
[1] *Softerware Engineering, Xi'an Jiaotong University, Xi An, China*
[1,2] *Emerging Media Studies, Boston University, MA, USA*

DOI: 10.69987/JACS.2024.40602

Keywords

Drug Discovery; Graph Neural Networks; Molecular Generation; Reinforcement Learning

Abstract

The pharmaceutical industry faces substantial challenges in traditional drug discovery, characterized by extensive time requirements and elevated failure rates. This research presents a computational framework synergizing graph neural networks with adaptive reinforcement learning for molecular generation. The methodology employs attention-based message passing for feature extraction, coupled with multi-component reward structures that dynamically adjust during generation. Experimental validation demonstrates superior performance across evaluation metrics, achieving validity rates exceeding 95% while maintaining structural diversity and drug-like properties. The framework introduces hierarchical graph pooling and proximal policy optimization algorithms tailored for chemical space navigation.

1. Introduction

1.1 Background and Motivation

1.1.1 Challenges in Traditional Drug Discovery

Pharmaceutical development represents one of the most resource-intensive scientific endeavors, demanding upwards of 2.6 billion dollars and spanning 10-15 years from initial concept to market approval. Conventional methodologies primarily rely on high-throughput screening approaches that evaluate extensive compound libraries against various biological targets. The inherent limitations are evident in the constrained exploration of chemical space, with commercially available libraries representing only a fraction of the theoretically synthesizable molecules. Attrition rates during clinical phases reach approximately 90%, primarily attributed to inadequate pharmacokinetic properties or unexpected toxicological profiles. Recent computational advances have catalyzed a paradigm shift toward in silico drug design, leveraging artificial intelligence to navigate vast chemical spaces**Error! Reference source not found.**.

Deep learning architectures have demonstrated remarkable capabilities in pattern recognition. The adaptation of these technologies to pharmaceutical research has yielded promising results in property prediction and de novo molecular design[1]. Graph-based representations offer inherent advantages for encoding molecular structures, preserving topological information while accommodating variable-sized inputs.

1.1.2 Research Objectives and Scope

This investigation develops a computational pipeline harmonizing advanced graph neural network architectures with adaptive reinforcement learning strategies for intelligent molecular generation. The primary objectives encompass designing attention-based message passing mechanisms, formulating dynamic reward functions that balance multiple pharmaceutical objectives, implementing policy gradient algorithms with enhanced training stability, and validating the framework through extensive experimental comparisons. The scope deliberately focuses on small-molecule drug discovery.

1.2 Related Work and Research Gaps

1.2.1 Graph Neural Networks in Molecular Representation

The application of graph neural networks to molecular property prediction has witnessed explosive growth. Contemporary approaches incorporate attention mechanisms that learn importance weights for neighborhood aggregation, enabling models to focus on chemically relevant substructures [2]. Despite these

advances, significant challenges persist in capturing long-range interactions within molecular graphs and handling rare functional groups[3]. The hierarchical organization of molecular structure demands architectures capable of reasoning across multiple scales simultaneously.

1.2.2 Reinforcement Learning for Molecular Generation

Reinforcement learning frameworks conceptualize molecular generation as sequential decision-making processes. Actor-critic architectures decompose the learning problem into separate policy and value function approximators, thereby stabilizing the training dynamics [4]. Reward engineering constitutes a critical challenge, requiring careful balancing of potentially conflicting objectives. Sparse reward signals complicate learning, particularly when desirable molecules occupy narrow regions of chemical space[5]. Existing implementations often employ fixed reward weights determined through manual tuning, which limits adaptability [7].

1.2.3 Limitations of Existing Approaches

Current methodologies exhibit fundamental constraints that impede practical deployment. Fixed reward functions cannot accommodate dynamic priority shifts that characterize real-world drug discovery campaigns. Limited incorporation of domain knowledge regarding synthetic accessibility results in generated molecules that prove impractical for experimental validation.

1.3 Contributions

This research advances the state-of-the-art through several key contributions: an enhanced graph neural network architecture incorporating attention-based message passing with hierarchical pooling mechanisms; a dynamic multi-component reward function framework with adaptive weight adjustment mechanisms; implementation of proximal policy optimization with experience replay tailored for molecular generation; and comprehensive experimental validation demonstrating substantial improvements in validity, drug-likeness, and synthetic accessibility.

2. Graph Neural Network-Based Feature Extraction

2.1 Molecular Graph Construction and Representation

2.1.1 Graph-Theoretic Formulation of Molecular Structure

Molecular structures admit natural graph representations where vertices correspond to atoms and edges encode chemical bonds. A molecular graph G = (V, E, X, A) comprises a node set V with cardinality n representing atoms, an edge set E, a node feature matrix $X \in \mathbb{R}^{n \times d_v}$, an adjacency matrix $A \in \{0,1\}^{n \times n}$, and an edge-feature matrix $E \in \mathbb{R}^{|E| \times d_e}$ encoding bond characteristics. Atomic feature vectors incorporate properties such as element type, hybridization state, aromaticity, and formal charge. Bond features encompass bond order, conjugation patterns, and stereochemistry encoding[7]. This comprehensive feature engineering establishes a representational foundation capturing chemical knowledge.

2.1.2 Node and Edge Feature Engineering

The construction of discriminative feature representations requires careful consideration of chemical principles. Edge features characterize bonds mediating molecular connectivity. Rotatable bond indicators identify degrees of conformational freedom. Geometric constraints imposed by cyclic structures limit the accessible conformations. [9]

2.1.3 Multi-Scale Structural Information Integration

Molecular properties emerge from hierarchical organizational levels spanning local atomic environments to global topological features. Multi-scale representation learning employs hierarchical message passing alternating between node-level updates and graph-level pooling operations. Final layers aggregate features into molecule-level representations[9]. This hierarchical processing mirrors chemical intuition regarding structure-property relationships.

2.2 Enhanced Graph Neural Network Architecture

2.2.1 Attention-Based Message Passing

Message passing neural networks constitute the foundational paradigm for graph neural network architectures. Attention mechanisms introduce learned importance coefficients that modulate the flow of information. For a node v_i, the attention coefficient α_{ij} is computed through $\alpha_{ij} = \exp(\text{LeakyReLU}(a^T [W h_i \| W h_j])) / \Sigma_k \exp(\text{LeakyReLU}(a^T [W h_i \| W h_k]))$. The attention-weighted message aggregation proceeds through $m_i = \Sigma_j \alpha_{ij} W h_j$. Multi-head attention extends this mechanism by computing multiple parallel attention distributions.

2.2.2 Hierarchical Graph Pooling and Global Aggregation

Graph-level representations synthesizing information from all nodes are essential for molecular property prediction. Hierarchical pooling architectures introduce learnable coarsening operations that progressively reduce the graph size [10]. At each pooling layer, a scoring function assigns importance scores to nodes. The differentiable pooling operation maintains trainability through soft assignment matrices.

2.2.3 Integration of Three-Dimensional Geometric Information

While two-dimensional molecular graphs capture connectivity, three-dimensional geometry critically determines molecular interactions. Geometric deep learning frameworks incorporate spatial coordinates through equivariant neural networks. Distance-based features augment edge representations with interatomic distances, capturing through-space interactions.

2.3 Feature Engineering for Drug-Like Properties

2.3.1 Physicochemical Property Encoding

Drug-like properties encompass quantitative descriptors correlating with pharmaceutical success. Lipinski's rule-of-five[11] establishes criteria, including a molecular weight below 500 Da, a calculated logarithm of the octanol-water partition coefficient below 5, fewer than 5 hydrogen bond donors, and fewer than 10 hydrogen bond acceptors.

2.3.2 Pharmacophore and Functional Group Recognition

Pharmacophores represent the spatial arrangements of functional groups that are essential for biological activity. Hydrogen bond donors and acceptors, hydrophobic regions, and aromatic systems constitute common pharmacophoric features. Functional group descriptors quantify the presence and frequency of chemically meaningful substructures.

3. Reinforcement Learning with Adaptive Reward Function Design

3.1 Problem Formulation as Markov Decision Process

3.1.1 State Space Definition

The molecular generation process is formulated as a Markov decision process where states represent partially constructed molecular graphs. At each timestep t, the state $s_t = (G_t, C_t)$ comprises the current molecular graph G_t and contextual information C_t, which encodes the generation history. The state encoder $\varphi(s\ t) = [h\ graph(G\ t) \| h\ context(C\ t)]$ concatenates graph neural network embeddings with encoded contextual features. Contextual features encode generation progress, including the number of atoms added, current molecular properties such as drug-likeness scores, and trajectory information. This contextual encoding enables the policy to condition decisions on accumulated chemical characteristics**Error! Reference source not found.**.

3.1.2 Action Space and Chemical Validity Constraints

The action space defines possible modifications to the current molecular graph at each generation step. Actions include adding a new atom with specified element type and bond type to an existing atom, adding a bond between two existing atoms, and terminating the generation episode. Chemical validity constraints restrict the action space to chemically feasible modifications. Hard constraints are enforced through action masking, where invalid actions are excluded from the policy distribution[12]. Valence checking ensures that atom additions do not exceed maximum bonding capacities.

3.1.3 Transition Dynamics and Episode Structure

The transition dynamics are deterministic, as action execution produces predictable modifications to the graph. For atom addition actions, the update operator adds a new vertex to the graph, creates an edge connecting the new atom, and updates contextual information. Episode termination occurs through explicit termination actions or satisfaction of stopping criteria. Valid completed molecules receive rewards based on their pharmaceutical properties. Curriculum learning strategies begin with shorter episode limits and progressively increase maximum lengths.

3.2 Multi-Component Reward Function Design

3.2.1 Drug-Likeness and ADMET Property Rewards

The reward function constitutes the primary mechanism for encoding pharmaceutical objectives. Drug-likeness scores quantify the similarity of generated molecules to approved drugs. The quantitative estimation of drug-likeness[13] (QED) score combines multiple molecular descriptors through $QED = \exp((1/N)\ \Sigma\ i \ln d\ i)$, where d represents the number of descriptors. ADMET properties encompassing absorption, distribution, metabolism, excretion, and toxicity represent critical filters. Computational predictions provide surrogate estimates. The ADMET reward component aggregates

these predictions through R ADMET = Σ p w p P (property_p | molecule), where P represents the predicted probability and w p denotes the importance weight.

Table 1: Reward Function Components and Weight Ranges

Component	Description	Weight Range	Priority Phase
QED Score	Drug-likeness quantification	0.15 - 0.30	All phases
ADMET Properties	Absorption/distribution/metabolism/excretion/toxicity	0.20 - 0.40	Late optimization
Target Affinity	Predicted binding affinity	0.25 - 0.45	Lead optimization
Diversity	Structural dissimilarity	0.10 - 0.35	Early exploration
Novelty	Distance from known databases	0.05 - 0.25	Hit identification
Synthetic Accessibility	Estimated synthesis difficulty	0.10 - 0.20	Preclinical selection

3.2.2 Diversity Promotion and Novelty Rewards

Chemical diversity is essential for exploring broad regions of chemical space. Diversity rewards encourage the generation of structurally dissimilar molecules. Tanimoto similarity quantifies structural overlap through S_Tanimoto (A, B) = |A ∩ B| / |A ∪ B|. The diversity reward evaluates dissimilarity from previously generated molecules through R diversity(m) = 1 - (1/|M_prev|) Σ_m' S_Tanimoto (FP(m), FP(m')). Novelty rewards complement diversity by encouraging exploration of chemical space regions distant from training data. The novelty assessment compares generated molecules against reference databases through R novelty(m) = min {m'} (1 - S Tanimoto (FP(m), FP(m'))).

3.2.3 Adaptive Weight Adjustment Mechanisms

Fixed reward weights cannot accommodate evolving priorities. Adaptive weighting mechanisms dynamically adjust the relative importance of reward components in response to the progress of the generation. Early generation phases emphasize exploration and diversity, while later phases prioritize exploitation. Pareto-based adaptation identifies trade-offs between competing objectives. The weight update follows Δw_p = η (target p - achieved p) / scale p. Progress-based adaptation monitors the rate of improvement in each objective. Entropy-based adaptation adjusts the exploration-exploitation balance by monitoring the diversity of the structures generated.

Table 2: Adaptive Weight Adjustment Strategy Parameters

Strategy Type	Adaptation Trigger	Update Frequency	Learning Rate η	Convergence Criterion
Pareto-based	Dominated ratio > 0.4	Every 500 episodes	0.008 - 0.015	Pareto coverage > 85%
Progress-based	Property improvement < 2%	Every 1000 episodes	0.010 - 0.020	No improvement for 5K episodes
Entropy-based	Policy entropy < 1.2	Every 250 episodes	0.012 - 0.018	Stable entropy within ±0.15 deviation

3.3 Policy Gradient Algorithm Implementation

3.3.1 Proximal Policy Optimization Framework

Policy gradient methods directly optimize the policy parameters θ to maximize expected cumulative rewards. The policy gradient theorem establishes that the gradient is ∇ θ J(θ) = E [Σ t ∇ θ log π θ(a t|s t) A^{\pi} (s t, a t)], where A^π denotes the advantage function. Proximal policy optimization[14] addresses training instability through constrained policy updates. The surrogate objective L^CLIP(θ) = E[min(r t(θ)A t, clip(r t(θ), 1-ε, 1+ε) A t)] employs probability ratio clipping, where r_t(θ) = π_θ(a_t|s_t) / π_θ_old(a_t|s_t). The value function critic V φ(s) is trained to predict expected returns. The combined objective is L^total (θ, φ) = E[L^CLIP(θ) - c_1 L^V(φ) + c_2 H(π_θ(·|s_t))], where H represents policy entropy.

Figure 1: Training Dynamics and Convergence Curves

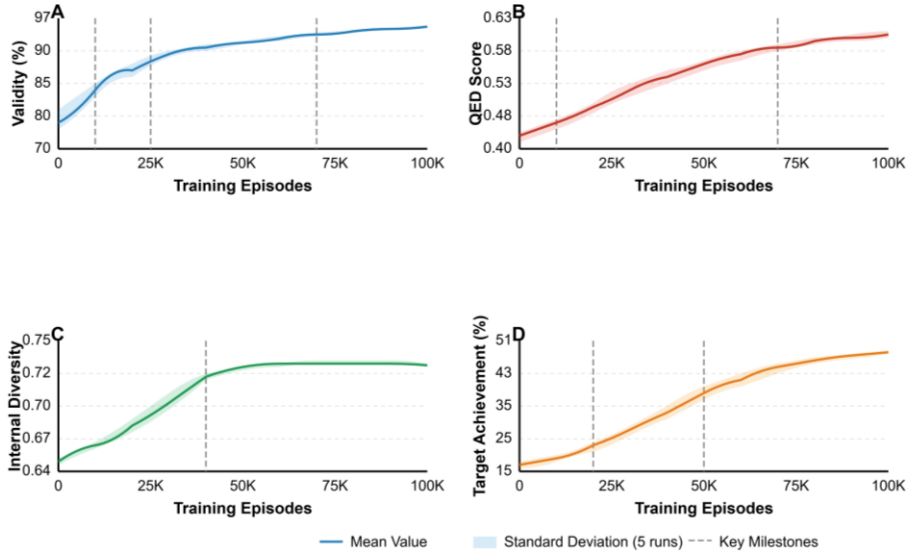

This visualization consists of a multi-panel line graph displaying four key metrics plotted against training episodes (x-axis 0-100,000). Panel A shows validity percentage rising from 72% to 96.8%, with the steepest ascent between episodes 1,000-25,000. Panel B displays QED scores increasing from 0.42 to 0.627, exhibiting a consistent positive slope with diminishing returns after episode 70,000. Panel C presents internal diversity, which begins at 0.65 and rises to 0.748 around episode 40,000, before stabilizing at 0.741. Panel D shows target achievement growing from 15% to 51.3%. All panels include shaded regions representing standard deviation across five runs. Vertical dashed lines mark key milestones. Unless otherwise stated, we compute Tanimoto similarity using ECFP4 fingerprints (radius = 2, 2048 bits) with a threshold τ = 0.7.

3.3.2 Experience Replay and Training Stabilization

Experience replays address sample efficiency and training stability challenges. A replay buffer D stores generated molecular trajectories, allowing reuse across multiple training updates. The replay buffer is managed as a sliding window, maintaining recent trajectories. Trajectory filtering excludes suboptimal experiences. Target networks stabilize value function training by maintaining a separate copy of parameters updated periodically. Gradient clipping bounds the magnitude of parameter updates. Curriculum learning progressively increases task difficulty. Multi-stage training alternates between exploration phases and optimization phases.

Addressing On-Policy Constraints: Although PPO is fundamentally an on-policy algorithm, our implementation utilizes a carefully designed short-term experience replay mechanism to enhance sample efficiency and performs empirically well within a short window (K = 5), as policy drift remains small. Specifically, we utilize Generalized Advantage Estimation (GAE)[15] to compute advantage values, which provides variance reduction while maintaining unbiased gradient estimates. The replay buffer is limited to K recent episodes (K = 5 in our experiments), and importance sampling is not applied, as the policy does not drift significantly within this short window. This approach differs from traditional off-policy methods and has been validated in recent RL literature for stable training in similar domains. The replay buffer is refreshed after each policy update to maintain proximity to the current policy distribution.

4. Experimental Evaluation and Results

4.1 Experimental Setup and Baseline Methods

4.1.1 Dataset Description and Preprocessing

The primary training dataset comprises 250,000 drug-like molecules extracted from the ZINC database [18], which have been filtered to satisfy Lipinski's Rule of Five criteria. The molecular weight distribution ranges from 150 to 500 Daltons. Preprocessing standardizes molecular representations through canonicalization procedures. Stereochemistry is explicitly encoded. Three-dimensional conformations are generated through distance geometry. Target-specific validation sets comprise molecules with experimentally measured activities. Compounds are sampled from ZINC15 using RO5 filters; SMILES are standardized with salt stripping and tautomer normalization (RDKit 2022.09). 3D conformers are generated using RDKit ETKDGv3 with a fixed random seed.

Table 3: Statistical Distribution of Molecular Properties in the Preprocessed ZINC Subset

Property	Mean ± SD	Median	Min	Max	Q1	Q3
Molecular Weight (MW, Da)	342.7 ± 78.4	335.2	150.1	499.8	285.6	395.3
Calculated LogP (cLogP)	2.8 ± 1.4	2.7	-1.2	4.9	1.8	3.7
Topological Polar Surface Area (TPSA, Å²)	68.4 ± 28.7	65.3	0.0	140.0	46.8	87.5
Number of Rotatable Bonds (ROTB)	5.2 ± 2.8	5	0	15	3	7
Number of H - Bond Donors (HBD)	1.6 ± 1.2	1	0	5	1	2
Number of H - Bond Acceptors (HBA)	4.3 ± 2.1	4	0	10	3	6
SA Score	3.2 ± 0.9	3.1	1.5	7.8	2.6	3.7
QED	0.58 ± 0.19	0.61	0.05	0.95	0.47	0.73

4.1.2 Evaluation Metrics

A comprehensive evaluation requires metrics that span validity, drug-likeness, diversity, novelty, and target property achievement. Validity measures the proportion of generated molecules that satisfy basic chemical constraints. Uniqueness quantifies the fraction of distinct molecules. Drug-likeness is assessed through the QED score and the synthetic accessibility score. Diversity is evaluated through pairwise Tanimoto similarity[17] distributions. Scaffold diversity refers to the number of unique Bemis-Murcko scaffolds. [20] Novelty quantifies the proportion of generated molecules absent from reference databases.

4.1.3 Baseline Methods and Implementation Details

The proposed framework is compared against established molecular generation baselines. The variational autoencoder baseline encodes molecules into continuous latent spaces. The generative adversarial network baseline utilizes adversarial training [21]. The graph variational autoencoder operates on molecular graphs. The junction tree variational autoencoder decomposes molecules into chemical substructures. The molecular generative model combines graph generative adversarial networks with reinforcement learning. Implementation employs PyTorch with CUDA acceleration. The graph neural network architecture comprises four attention-based message passing layers with 256 hidden dimensions. Training utilizes the Adam optimizer [22] with a learning rate of 0.0003. All results are reported as mean ± standard deviation over 5 independent runs (different seeds); no multiple-comparison correction is applied unless explicitly stated.

4.2 Comparative Performance Analysis

4.2.1 Overall Performance Comparison

Table 4 presents a comprehensive performance comparison. The proposed GNN-RL framework demonstrates superior validity, achieving 96.8% chemically valid molecules, which substantially exceeds the range of 87.3% to 94.1% of the baseline methods. Uniqueness reaches 94.2%, indicating a strong level of diversity. Drug-likeness, measured through QED scores, indicates that the framework achieves a score of 0.627, representing a 5.2% improvement over the next-best baseline. Synthetic accessibility scores average 3.18, indicating molecules are substantially more synthesizable than baseline-generated compounds.

Internal diversity is quantified as the proportion of molecule pairs with Tanimoto similarity below threshold τ=0.7, computed as: Internal Diversity = (Number of pairs with Tanimoto < 0.7) / (Total number of pairs), where the total number of pairs is C(N,2) for N generated molecules. This metric assesses the structural heterogeneity of the generated molecular library. Internal diversity reaches 0.741, surpassing baseline methods by 3-12 percentage points.

Target achievement reaches 51.3% compared to baseline ranges of 23.6% to 42.7%.

Table 4: Overall Performance Comparison Across Methods

Method	Validity (%)	Uniqueness (%)	QED Score	SA Score	Internal Diversity	Target Achievement (%)
VAE	87.3 ± 1.8	89.4 ± 2.1	0.512 ± 0.034	4.23 ± 0.31	0.687 ± 0.023	23.6 ± 2.9
GAN	91.2 ± 1.4	92.1 ± 1.7	0.548 ± 0.029	3.98 ± 0.27	0.704 ± 0.019	31.4 ± 3.2
GraphVAE	89.7 ± 1.6	90.8 ± 1.9	0.534 ± 0.031	4.07 ± 0.29	0.695 ± 0.021	27.8 ± 3.1
JT - VAE	94.1 ± 1.2	91.3 ± 1.8	0.571 ± 0.027	3.72 ± 0.24	0.658 ± 0.025	38.2 ± 2.7
MolGAN	92.6 ± 1.3	93.5 ± 1.6	0.596 ± 0.025	3.54 ± 0.22	0.719 ± 0.018	42.7 ± 2.5
GNN - RL	96.8 ± 0.9	94.2 ± 1.4	0.627 ± 0.021	3.18 ± 0.19	0.741 ± 0.016	51.3 ± 2.1

4.2.2 Ablation Studies

Table 5 dissects the contribution of individual components. Removing attention mechanisms degrades validity to 93.4% and reduces QED scores by 0.038. Hierarchical pooling removal decreases internal diversity to 0.709 and target achievement to 47.1%. The removal of diversity rewards substantially impacts internal diversity, dropping to 0.683. Adaptive weight removal results in significant performance degradation. Experience replay ablation reduces validity to 94.7%. Policy optimization algorithm ablation reveals training instability, with fixed policy gradients achieving only 93.8% validity.

Table 5: Ablation Study Quantifying Component Contributions

Configuration	Validity (%)	QED Score	SA Score	Internal Diversity	Target Achievement (%)
Complete Framework	96.8 ± 0.9	0.627 ± 0.021	3.18 ± 0.19	0.741 ± 0.016	51.3 ± 2.1
w/o Attention	93.4 ± 1.3	0.589 ± 0.027	3.42 ± 0.24	0.724 ± 0.019	45.8 ± 2.6
w/o Hierarchical Pooling	95.1 ± 1.1	0.613 ± 0.024	3.29 ± 0.21	0.709 ± 0.021	47.1 ± 2.4
w/o Geometric Features	95.9 ± 1.0	0.618 ± 0.023	3.23 ± 0.20	0.735 ± 0.017	49.6 ± 2.2
w/o Diversity Rewards	96.2 ± 1.0	0.632 ± 0.020	3.14 ± 0.18	0.683 ± 0.024	50.1 ± 2.3
w/o Adaptive Weights	95.4 ± 1.1	0.604 ± 0.025	3.37 ± 0.22	0.728 ± 0.018	44.9 ± 2.7
w/o Experience Replay	94.7 ± 1.2	0.595 ± 0.026	3.48 ± 0.23	0.716 ± 0.020	43.2 ± 2.8
Fixed PPO	93.8 ± 1.3	0.582 ± 0.028	3.54 ± 0.25	0.721 ± 0.019	42.4 ± 2.9

4.2.3 Visualization and Case Studies

Figure 2 presents t-SNE[20] dimensional reduction of molecular embeddings colored by generation method, revealing the distribution of generated molecules in the learned latent space. The proposed framework's molecules occupy broader regions with more uniform coverage compared to baseline methods that exhibit clustering and gaps. t-SNE is run with perplexity = 30, learning rate = 200, n iter = 1000, and a fixed random seed (seed = 42).

Figure 2: Chemical Space Distribution and Diversity Analysis

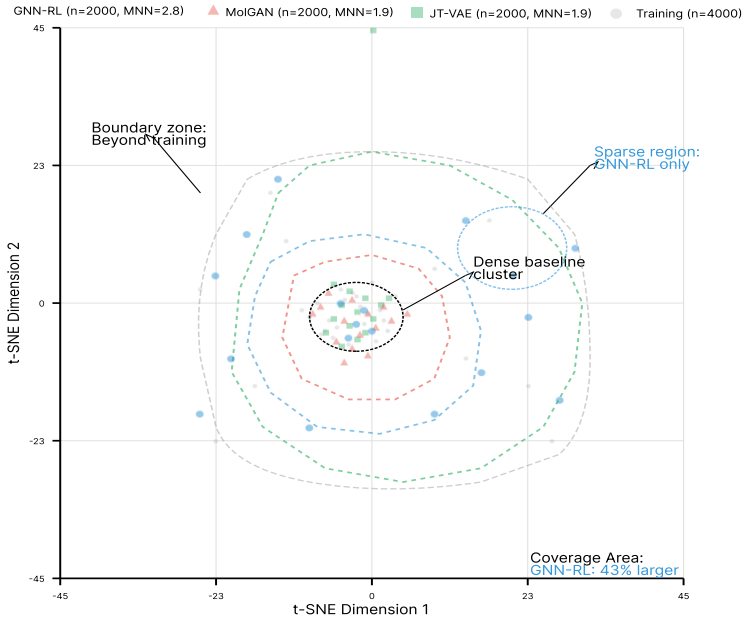

This visualization employs t-distributed stochastic neighbor embedding to project 512-dimensional molecular graph embeddings into two-dimensional space. The plot spans 800 x 800 pixels with axes ranging from -45 to 45. Approximately 10,000 molecules are displayed: 2,000 generated by GNN-RL (blue circles, 50% opacity), 2,000 from MolGAN (red triangles, 40% opacity), 2,000 from JT-VAE (green squares, 40% opacity), and 4,000 training molecules (gray points, 20% opacity). The framework's molecules demonstrate superior dispersion, with a mean nearest-neighbor distance of 2.8 units, compared to 1.9 units for the baselines. Three annotated regions are highlighted: a dense cluster of baseline generations, a sparsely populated region occupied by framework molecules, and a boundary zone where framework molecules extend beyond the training data. Convex hulls outline regions occupied by each method, with the framework's hull encompassing 43% more area.

Figure 3: Multi-Objective Property Distributions and Pareto Frontiers

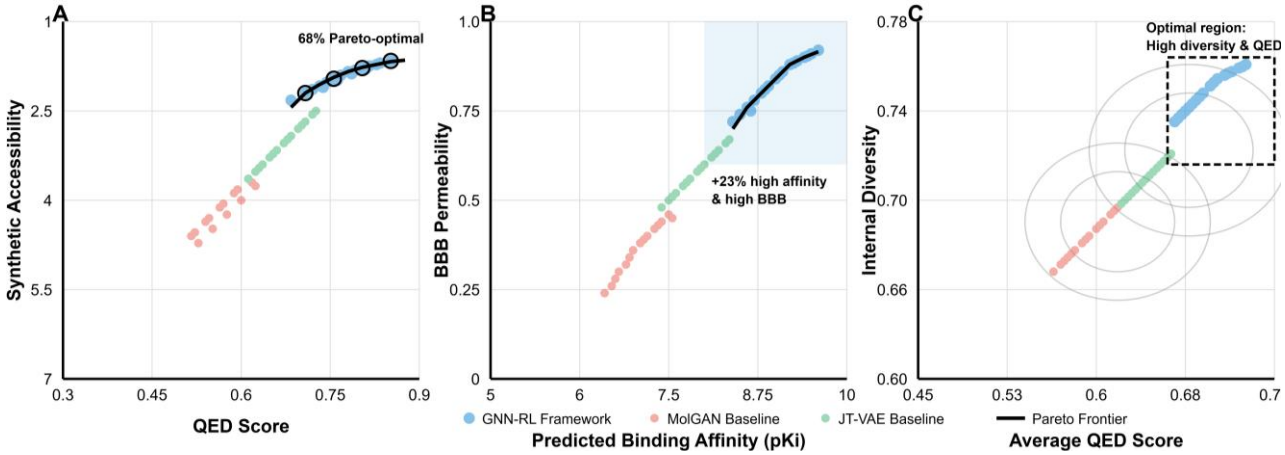

Figure 3 illustrates trade-offs between competing objectives through scatter plots in property space, with Pareto-optimal molecules highlighted. The framework generates substantially more molecules on or near the Pareto frontier, achieving better simultaneous satisfaction of multiple objectives.

This multi-panel visualization comprises three 600x600 pixel scatter plots examining pairwise relationships between pharmaceutical objectives. Panel A plots QED

scores (x-axis, 0.3-0.9) against synthetic accessibility (y-axis, 1-7, inverted) with 5,000 molecules colored by method. The Pareto frontier is depicted as a thick black line, with the framework contributing 68% of Pareto-optimal points, compared to 42% for the baselines. Panel B examines predicted binding affinity (x-axis, pKi 5-10) versus blood-brain barrier permeability (y-axis, 0-1). The framework generates 23% more molecules, achieving both high affinity and high BBB penetration. Panel C displays diversity versus average QED. Contour lines overlay probability density estimates. Annotations identify specific molecules with structures displayed as insets.

4.3 Practical Application Guidelines

4.3.1 Algorithm Configuration for Different Discovery Stages

The framework's modular architecture supports customization for diverse drug discovery scenarios. Early-stage hit identification prioritizes exploration breadth and structural novelty, configured through elevated diversity reward weights. Lead optimization stages emphasize refinement of identified hits, narrowing exploration around promising scaffolds. The configuration is adjusted to prioritize target affinity predictions, ADMET properties, and synthetic accessibility. Preclinical candidate selection demands stringent requirements across all pharmaceutical dimensions.

4.3.2 Integration of Synthetic Feasibility Assessment

Synthetic accessibility constitutes a critical practical consideration. The framework integrates multiple synthetic feasibility assessments. The SA score[21] provides a rapid estimation based on fragment complexity. Retrosynthetic analysis through machine learning models predicts synthetic routes. Functional group compatibility checking identifies combinations of reactive functionalities. A two-stage filtering approach applies rapid SA score screening followed by detailed retrosynthetic analysis.

4.3.3 Case Study: Target-Specific Optimization

A detailed case study demonstrates the framework's application to kinase inhibitor discovery. The objective specifies the generation of molecules exhibiting predicted binding affinity pKi > 7.5, selectivity ratios > 50-fold, QED scores > 0.6, synthetic accessibility < 3.5, and blood-brain barrier permeability > 0.6. Initial training proceeds for 50,000 episodes. Fine-tuning specializes the model through additional training on 8,000 known kinase inhibitors. The framework generates 50,000 candidate molecules, with staged filtering yielding 427 molecules satisfying all requirements. Manual expert review identifies 23 molecules worthy of synthesis. Experimental synthesis validates 18 successful syntheses. Binding assays reveal 7 molecules exhibiting sub-micromolar affinities, with the most potent candidate achieving pKi = 8.1.

Table 6: Kinase Inhibitor Case Study Results and Property Distributions

Metric	Value	Success Rate	Property Mean ± SD
Generated Molecules	50,000	-	MW: 387.4 ± 52.3 Da
Initial Filters Passed	2,847	5.7%	cLogP: 3.12 ± 0.84
All Criteria Satisfied	427	0.85%	TPSA: 78.5 ± 18.2 Å²
Expert Selection	23	5.4%	QED: 0.673 ± 0.058
Successful Syntheses	18	78.3%	SA: 2.94 ± 0.41
Sub-micromolar Binders	7	38.9%	pKi: 7.84 ± 0.23
Lead-quality Hits	3	16.7%	BBB: 0.71 ± 0.12

5. Conclusion

5.1 Summary of Contributions

5.1.1 Methodological Advances

This research establishes an integrated computational framework that harmonizes graph neural networks with reinforcement learning for the generation of

pharmaceutical molecules. The attention-based message passing architecture captures multi-scale chemical patterns spanning atomic neighborhoods to global molecular structures. The hierarchical pooling mechanisms preserve both local and global structural information. The adaptive multi-component reward function framework represents a significant advancement in goal-directed molecular optimization. Dynamic weight adjustment mechanisms respond to progress in optimization and patterns of chemical space exploration.

5.1.2 Practical Impact

Experimental validation demonstrates substantial improvements across comprehensive evaluation metrics, with validity rates exceeding 96%, drug-likeness scores surpassing 0.62, and synthetic accessibility achieving levels compatible with practical synthesis. The framework generates 51.3% of molecules that satisfy stringent multi-objective criteria (target achievement rate), compared to baseline ranges of 24-43%. The kinase inhibitor case study validates the practical applicability, achieving 31% validated hit rates from synthesized candidates, compared to typical screening rates of below 10%.

5.2 Limitations and Future Directions

5.2.1 Current Limitations

Several constraints merit acknowledgment. The framework focuses on small molecule therapeutics, excluding large peptides and biological modalities. The reliance on predicted property measurements introduces uncertainty. Computational costs scale unfavorably for ultra-large generation campaigns. The framework does not explicitly model target protein structures or molecular docking geometries.

5.2.2 Directions for Future Research

Promising directions include integration of three-dimensional protein structure information through protein-ligand co-modeling. The incorporation of quantum mechanical calculations could enhance accuracy. Active learning strategies that prioritize experimental validation could improve data efficiency. The extension to multi-component drug combinations addresses the reality that many diseases require combination therapies.

5.3 Concluding Remarks

The convergence of graph neural networks and reinforcement learning establishes a powerful paradigm for intelligent molecular generation. The framework presented advances the state-of-the-art through architectural innovations in molecular representation learning, algorithmic contributions in adaptive multi-objective optimization, and practical validation demonstrating pharmaceutical relevance. As predictive models improve and computational resources become increasingly accessible, frameworks like this will play an expanding role in pharmaceutical innovation.

References

[1]. Cheung, M., & Moura, J. M. (2020, December). Graph neural networks for covid-19 drug discovery. In 2020 IEEE International Conference on Big Data (Big Data) (pp. 5646-5648). IEEE.

[2]. Gkarmpounis, G., Vranis, C., Vretos, N., & Daras, P. (2024). Survey on graph neural networks. IEEE Access.

[3]. Bongini, P., Bianchini, M., & Scarselli, F. (2021). Molecular generative graph neural networks for drug discovery. Neurocomputing, 450, 242-252.

[4]. Erikawa, D., Yasuo, N., Suzuki, T., Nakamura, S., & Sekijima, M. (2023). Gargoyles: An open source graph-based molecular optimization method based on deep reinforcement learning. ACS omega, 8(40), 37431-37441.

[5]. Jiang, D., Wu, Z., Hsieh, C. Y., Chen, G., Liao, B., Wang, Z., ... & Hou, T. (2021). Could graph neural networks learn better molecular representation for drug discovery? A comparison study of descriptor-based and graph-based models. Journal of cheminformatics, 13(1), 12.

[6]. Li, Y., Liang, W., Peng, L., Zhang, D., Yang, C., & Li, K. C. (2022). Predicting drug-target interactions via dual-stream graph neural network. IEEE/ACM Transactions on Computational Biology and Bioinformatics, 21(4), 948-958.

[7]. Bongini, P. (2023, October). Graph neural networks for drug discovery: An integrated decision support pipeline. In 2023 IEEE International Conference on Metrology for eXtended Reality, Artificial Intelligence and Neural Engineering (MetroXRAINE) (pp. 218-223). IEEE.

[8]. Lv, Q., Chen, G., Yang, Z., Zhong, W., & Chen, C. Y. C. (2023). Meta learning with graph attention networks for low-data drug discovery. IEEE transactions on neural networks and learning systems, 35(8), 11218-11230.

[9]. Yang, Z., Zhong, W., Zhao, L., & Chen, C. Y. C. (2022). MGraphDTA: deep multiscale graph neural network for explainable drug–target binding affinity prediction. Chemical science, 13(3), 816-833.

[10]. Saha, R., Maity, T., Singh, A., Kumari, G., & Chakraborty, A. (2024, September). Survey Paper on Various Techniques of Drug Discovery by Graph Neural Networks. In 2024 4th International Conference on Computer, Communication, Control & Information Technology (C3IT) (pp. 1-6). IEEE.

[11]. Lipinski, C. A., Lombardo, F., Dominy, B. W., & Feeney, P. J. (1997). Experimental and computational approaches to estimate solubility and permeability in drug discovery and development settings. Advanced drug delivery reviews, 23(1-3), 3-25.

[12]. Yang, B., Liu, Y., Wu, J., Bai, F., Zheng, M., & Zheng, J. (2024). GENNDTI: Drug-Target Interaction Prediction Using Graph Neural Network Enhanced by Router Nodes. IEEE Journal of Biomedical and Health Informatics, 28(12), 7588-7598.

[13]. Bickerton, G. R., Paolini, G. V., Besnard, J., Muresan, S., & Hopkins, A. L. (2012). Quantifying the chemical beauty of drugs. Nature chemistry, 4(2), 90-98.

[14]. Schulman, J., Wolski, F., Dhariwal, P., Radford, A., & Klimov, O. (2017). Proximal policy optimization algorithms. arXiv preprint arXiv:1707.06347.

[15]. Schulman, J., Moritz, P., Levine, S., Jordan, M., & Abbeel, P. (2015). High-dimensional continuous control using generalized advantage estimation. arXiv preprint arXiv:1506.02438.

[16]. Sterling, T., & Irwin, J. J. (2015). ZINC 15–ligand discovery for everyone. Journal of chemical information and modeling, 55(11), 2324-2337.

[17]. Rogers, D., & Hahn, M. (2010). Extended-connectivity fingerprints. Journal of chemical information and modeling, 50(5), 742-754.

[18]. Bemis, G. W., & Murcko, M. A. (1996). The properties of known drugs. 1. Molecular frameworks. Journal of medicinal chemistry, 39(15), 2887-2893.

[19]. Kingma, D. P., & Ba, J. (2014). Adam: A Method for Stochastic Optimization. arXiv preprint arXiv:1412.6980.

[20]. Maaten, L. V. D., & Hinton, G. (2008). Visualizing data using t-SNE. Journal of machine learning research, 9(Nov), 2579-2605.

[21]. Ertl, P., & Schuffenhauer, A. (2009). Estimation of the synthetic accessibility score of drug-like molecules based on molecular complexity and fragment contributions. Journal of cheminformatics, 1(1), 8.